Pore-Scale Controls on Reaction-Driven Fracturing

Anja Røyne and Bjørn Jamtveit

Physics of Geological Processes (PGP)
Departments of Physics and Geoscience
University of Oslo
P.O. Box 1048
Blindern
N-0316 Oslo
Norway

anja.royne@fys.uio.no

bjorn.jamtveit@geo.uio.no

INTRODUCTION

Fluid migration through reactive rocks invariably leads to modifications of the rock porosity and pore structure. This, in turn, provides feedback on the fluid migration process itself. Reactions may lead to increases or decreases of the rock permeability. When the volume of solids decreases, either by an increase in the rock density or by transport of mass out of the system, the corresponding increase in porosity will enhance fluid transport and the continued propagation of the reaction front (Putnis 2015, this volume). In contrast, reactions that increase the solid volume will fill the pore space and may reduce permeability (Hövelmann et al. 2012). In this case, the reaction will only proceed if the stress generated by the volume-increasing process is large enough to create a fracture network that will enable continued fluid flow. Reaction-induced fracturing is particularly relevant during fluid migration into high-grade metamorphic and slowly cooled magmatic rocks with very low initial porosity, but may also be important during reactive transport in more porous rocks where growth processes within the pore space exerts forces on the pore walls (Jamtveit and Hammer 2012).

In this article we attempt to shed some light on the factors that determine whether volume-increasing reactions and growth in pores will reduce or increase permeability. We will start by describing field-scale examples of reaction-driven fracturing, and use a Discrete Element Model (DEM) to analyze how the resulting pattern and the rate and progress of reaction depend on the initial porosity of the rock. Ultimately, however, stress generation is related to growth processes taking place at the pore scale. We will therefore zoom in and describe pore-scale growth processes and how these are associated with fracturing and the production of new reactive surface area and new transport channelways for migrating fluids.

Stress generation by growth in pores requires that crystals continue to grow even after having 'hit' the pore wall. This implies that the fluid from which the crystals precipitate is not squeezed out from the reactive interface by the normal stress generated by the growth, but can be kept in place as a thin film by opposing forces that operate at very small scales. To understand the dynamics of crystal growth against confining pore walls, we need to zoom in even further and examine interface processes taking place at the nanometer scale. Hence, the last part of this chapter focuses on the nanometer-scale morphology of the reacting interface and the mechanical and transport properties of the fluids confined along reactive grain boundaries.

FIELD-SCALE OBSERVATIONS

Reaction-induced fracturing: The effect of porosity

The potential importance of reaction-driven fracturing is highest when the confining pressure is low or the rock is under high differential stress. In such a situation, even modest reaction-driven stresses may cause failure and fracture propagation. Spheroidal weathering is an example of a process where reactions produce pronounced fracturing under the low confining pressures that prevail near the Earth's surface (Fletcher et al. 2006; Røyne et al. 2008). This kind of weathering has been described for most rock types in a wide range of climate zones (Chapman and Greenfield 1949). Although spheroidal weathering, per definition, involves surface-parallel fracturing and spalling of layers at the margin of rock blocks, which become progressively rounded (core stones), the progress of this mode of weathering and the fracture patterns produced are sensitive to the initial porosity of the rock type, as outlined below.

A representative example of spheroidal weathering of a rock with very low initial porosity is shown in Figure 1. Interactions between the dolerite and oxidizing groundwaters generate a characteristic sequence of mm-to-cm-thick spalls that separates the weathered product from almost completely fresh dolerite. During progressive weathering, the central core stone will often split into two or more daughter core stones by a process called twinning. This process is also driven by the stresses generated through the volume-increasing reactions at the outer margin of the fresh core stone (Røyne et al. 2008). Because rocks are elastically extremely stiff, only a very small volume change «1% may generate stresses high enough to crack the rock.

Figure 2 shows spheroidal weathering of an andesitic intrusion with an original porosity of ~8% (Jamtveit et al. 2011). During spheroidal weathering, reaction-driven expansion and spalling occur along with domain-dividing fractures to form smaller "twins" and "triplets". In contrast to the situation described for the dolerite above, there are no sharp reaction fronts or interfaces, and individual core stones show pronounced progress of weathering reactions tens of centimeters inside the innermost onion-skin fracture. In fact, most core stones show significant production of weathering products in the pores throughout the entire rock volume, with no remaining completely unaltered andesite.

Figure 1. Spheroidal weathering of doleritic sill intrusion from the Karoo Basin, South Africa. Reaction-driven fracturing produces a number of spalls ('onion-skin'-like fractures) that result in a rounded 'core stone' from an initially angular dolerite block, cut out by pre-existing joints (left). Continued weathering eventually produces tensile stresses inside the core stone that are high enough to make the original core stone (outlined by solid lines) divide into two or more daughters (dashed lines) (right). [Modified from Røyne et al. 2008].
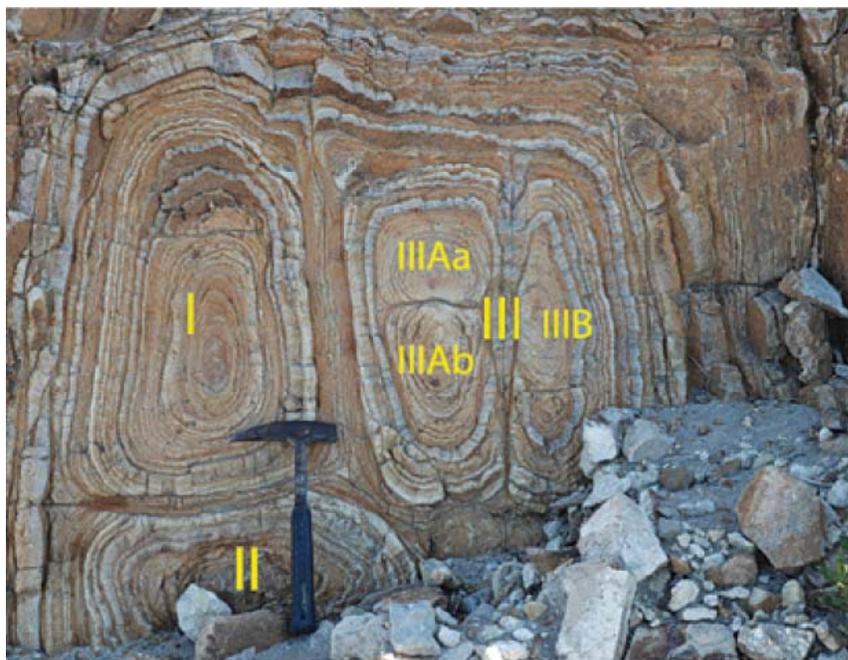
Figure 2. Block of an andesitic intrusion subdivided into smaller domains (I–III) by internal fracturing. Domain III was further subdivided into IIIA and IIIB, before IIIA split into twins IIIAa and IIIAb. The brown-colored striation is a combination of Liesegang bands and onion-skin fractures. [Modified from Jamtveit et al. 2011].

Recent numerical simulations have provided us with a more complete understanding of the differences described above. Until recently, most models focused on rocks with very low initial porosity where transport in unreacted rock occurred mainly by slow grain boundary diffusion. In such systems, a sharp reaction front separates completely unreacted rocks from rocks with a high extent of reaction. Moreover, the (1-D) propagation rate of this front is controlled mainly by the transport properties of the unfractured fresh rock (Rudge et al. 2010). However, in more porous rocks, the transport rates in unreacted rocks will be fast compared to the chemical reaction kinetics, and the reaction fronts may become broader with a more gradual transition from extensively reacted rock to fresh rock.

A 2-D model describing reaction-driven fracturing of rocks with variable porosity was recently presented by Ulven et al. (2014a). This model is a discrete element model (DEM) with a reaction-diffusion solver developed by Ulven et al. (2014b). It simulates the deformation and fracturing of a solid with constant intergranular porosity undergoing a local volume-increasing chemical reaction. Fluid flow in fractures is assumed to be effectively instantaneous compared to the rate of other relevant processes. In a natural system, the progress of the fluid-driven, volume-increasing reactions, as described by the model above, is controlled by two main parameters: rock porosity (Φ), and the shape of the initial domain undergoing volatilization. For the circular domains shown in Figure 3, porosity variation will control both the relative rates of reaction kinetics and transport, often expressed by the dimensionless Damkohler number ($\Gamma \propto 1/\Phi$), and the amount of the mobile reactant that the rock can contain ($\Theta \propto \Phi$). High porosity implies low Γ and high Θ (see Ulven et al. 2014a).

Figure 3 shows plots of reaction progress versus time for four different porosities, as well as fracture patterns developed at 50% reaction progress. As demonstrated by Ulven et al. (2014a), for porosities less than about 2.5%, the 'overall' reaction rate (rate averaged over the entire domain) is proportional to Φ^N, where N is in the range 0.45–2 and high N-values

(high sensitivity to initial porosity) corresponds to reactions with small volume changes. For initial porosities greater than 2.5%, the overall rate becomes increasingly less sensitive to the porosity, and is controlled mainly by the kinetics of the reaction.

In a natural system, the shape of the domains undergoing reaction will always deviate from a circle or a sphere. This has some important consequences for the reaction progress, as sharp edges or other regions with high curvature tend to act as foci for differential stress and thus control the timing of the onset of fracturing. Figure 4 shows examples of fracture patterns and reaction progress at 50% reaction for an initial porosity of 0.05%. This figure indicates that the total reaction rates are fairly similar after fracturing has commenced. However, the onset of fracturing (the steep part of the curves) is significantly different for different geometries. One implication of this is that spheroidal weathering of jointed rocks may progress very differently in blocks of different shape. Reaction-driven fracturing is thus expected to produce a characteristic size distribution of the resulting core stones as described by Fletcher and Brantley (2010) and Ulven et al. (2014a).
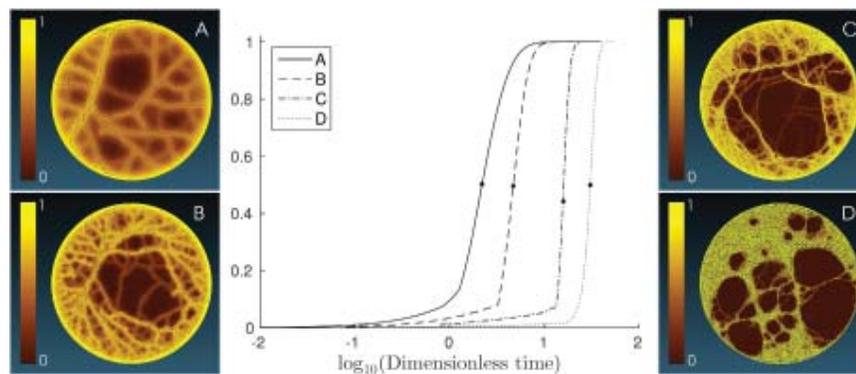
Figure 3. Total reaction progress versus time (central graph) for four different porosities: (A) $\Phi = 2.5\%$, (B) $\Phi = 0.9\%$, (C) $\Phi = 0.3\%$, and (D) $\Phi = 0.05\%$. Shade shows extent of reaction, from dark for unreacted material to light for completely reacted material Panels show fracture patterns and local reaction progress at 50% total reaction for systems with fluid flow in the fractures. The volume change of the reaction was 0.8% in all cases. [Modified from Ulven et al. 2014a].
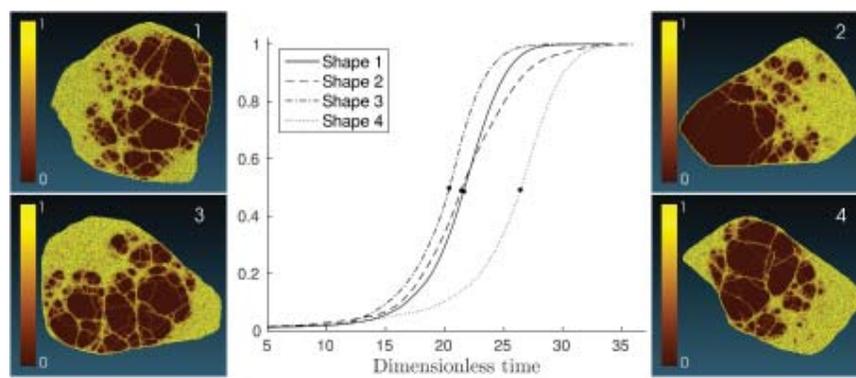
Figure 4. Reaction progress versus time for four different initial shapes (central graph). The panels show the four different domains (1-4) at 50% reaction progress for an initial porosity of 0.05%. [Modified from Ulven et al. 2014a].

Reaction-induced clogging and closure of fluid pathways

Although reactions may produce fractures and porosity, mineral growth in pores may also lead to clogging. This may significantly decrease the permeability and therefore fluid migration through initially porous rocks, and through rocks that are initially fractured due to tectonic and thermal processes. Tectonic deformation may, according to the Gutenberg–Richter law, riddle the crust with fractures on all scales (Molnar et al. 2007), and provide pervasive permeability and reactive surface area in brittly deformed rocks. When fluid-consuming reactions occur synchronously with tectonic deformation, the externally imposed stress may completely control the reaction rate and progress if permeability is generated at a faster rate than the infilling of pores by reaction products. On the other hand, if the precipitation rate is fast compared to the rate of fracturing and permeability generation, the progress of reaction may be modest even in extensively fractured rocks. Figure 5 shows a possible example of such a system: an extensively faulted, fractured, but only partly serpentinized, dunite.

Figure 5. Extensively fractured, faulted, and partly serpentinized dunite from the Leka ophiolite complex, Central Norwegian Caledonides. Despite the extensive fracturing and faulting observed, the average extent of serpentinization varies from 40–50 to 70–80% in the various domains of this outcrop.

Extrapolation of the kinetic data of the serpentinization reaction based on powder experiments (Malvoisin et al. 2012) predicts that hydration of the original rock should be complete within tens of years, a nearly instantaneous process on the time scales of plate tectonics. Yet, the extent of reaction is only about 50%. Clearly, the supply of water to the olivine surfaces must have been limited, in spite of the extensive fracturing process. Continuous clogging of thermally and tectonically induced fractures related to the strong increase in solid volume associated with the rapid olivine hydration reaction (> 30%) is a possible explanation for this observation (Malvoisin and Brunet 2014).

PORE-SCALE MECHANISMS

We will now take a closer look at the pore-scale mechanisms that lead to the stresses and fracture patterns discussed in the preceding section. The key requirement for reactions to take place is that water has access to the reactive surface. In the examples given below, we will show how fracturing can allow the reaction to proceed, and how the closure of nanoscale fluid pathways will cause the reaction to stop.

In all of these examples, two conditions are absolutely necessary for fracturing to take place. The first is some thermodynamic overstepping of the reaction. In geological settings, reactions are often assumed to take place very close to equilibrium. This cannot, however, lead to reaction-driven fracturing. The minimal (Griffith) requirement for fracture propagation to take place is that the elastic strain energy released during fracture propagation is at least equal to the amount of energy required to form two new fracture surfaces (Fletcher et al. 2006; Røyne et al. 2011b). When growing minerals perform work on their surroundings by displacing their confining walls, elastic strain energy builds up in the system. This energy comes from the chemical energy available in the reaction, and it requires that minerals precipitate from a supersaturated solution or that the Gibbs free energy, ΔG, of the reaction is sufficiently negative. As a crystal grows against the confinement of neighboring minerals, the stress on the growing crystal surface will increase. When the energy penalty for growing a crystal under normal stress becomes larger than the energy gained by precipitating material, growth will cease (Gibbs 1876; Steiger 2005a). The thermodynamic overstepping of the reaction therefore gives an upper bound for the mechanical stresses that can be generated from it.

The second prerequisite is the continued supply of reactants to the reaction site. In order to form a fracture, the material must be mechanically strained, meaning that the volume inside a pore must continuously increase until the strain is large enough for the fracture threshold to be reached. This requires that reactants must be transported to the reacting site while the reaction is taking place, even after the precipitated material has filled the original pore space. Since transport through solid phases is usually much too slow to be relevant, this transport must take place through a liquid film that is confined at the reactive interface, despite the normal stress that builds up across this interface (Taber 1916; Espinosa Marzal and Scherer 2008). Nanometer-thick confined fluid films can in many cases sustain significant normal stresses across them without being squeezed out. The normal stress is sustained by the disjoining pressure of the confined fluid film, which is a function of the film thickness (de Gennes et al. 2003; Israelachvili 2011). The maximum disjoining pressure depends on the details of the fluid and its confining surfaces, as will be further described in the last part of this chapter.

Fracturing around expanding grains

As demonstrated by Jamtveit et al. (2008), the swelling associated with olivine hydration may cause fracturing and a concomitant permeability increase (Fig. 6). In the upper 10 km of the Earth's crust, olivine hydration may produce stresses exceeding 300 MPa, greater than that required to fracture rocks, overcome the compressive stress, and cause frictional failure (Kelemen and Hirth 2012). However, in a ductile matrix, stresses may be released through creep processes that are not necessarily associated with significant permeability generation. Thus, serpentinization of olivine may be a more effective mechanism in generating fluid pathways in a rock when the olivine grains are surrounded by a brittle matrix than in a rock containing an increasing amount of mechanically weak serpentine minerals that may accommodate volume changes in a ductile manner.

Without this fracturing, grains that were not connected to a pre-existing fracture network would be virtually inaccessible to fluids. The reaction would then not be able to proceed, even though, thermodynamically, the olivine grains are out of equilibrium with the fluids that percolate through the rock.
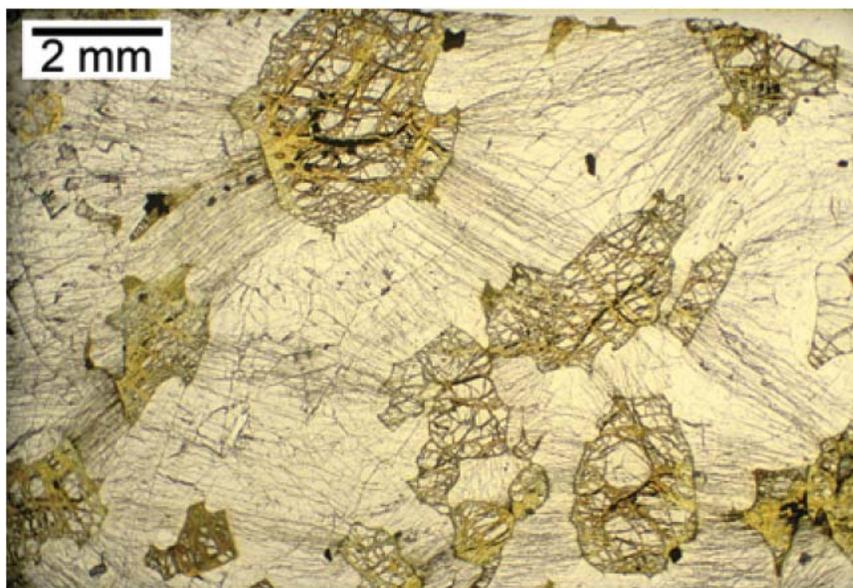
Figure 6. Micrograph of reaction-driven fracturing around partly serpentinized olivine crystals in a plagioclase matrix from a troctolite from the Duluth Igneous Complex. A dense network of microfractures connects individual olivine crystals and provides permeable pathways for fluid migration. Small olivine grains in unfractured regions are virtually unaltered [Reprinted from Jamtveit B, Malthe-Sørenssen A, Kostenko O, Reaction enhanced permeability during retrogressive metamorphism, *Earth and Planetary Science Letters,* Vol. 267, p. 620–627, Copyright (2008), with permission from Elsevier].

Intragrain fracturing

In nature, some volume-expanding reactions are very efficiently shut down by the formation of an impenetrable layer of precipitated mineral on the surface of the reactive grain (Prieto et al. 2003). The newly formed layer will be in equilibrium with the surrounding fluid, and the reactive grain is inaccessible to the fluids.

However, it is common for volume-expanding reactions to proceed to near or full completion. This may happen if the reaction causes fracturing of the reactive grain. Fracturing exposes new reactive surface and allows access to unreacted parts of the grain, thereby greatly accelerating the process. The fracturing of the reacting mineral grain is essential for the progress of any volume-increasing reaction, including almost all volatilization reactions. Without the continuous generation of new reactive surface area by fracturing, such reactions will normally result in the formation of a passivating layer of product phase and very limited reaction progress.

Replacement reactions mediated by a fluid phase take place through a coupled dissolution–precipitation reaction (Putnis 2002). When fluid comes into contact with the reactive mineral, dissolution takes place at the mineral surface. This immediately creates a supersaturated solution with respect to the replacing mineral, which will then precipitate in the immediate vicinity of the dissolving surface. A nanometer-scale confined fluid film between the parent and daughter phases will allow the reaction to continue. If the supersaturation with respect to the precipitating phase is high, there will be enough chemical energy available for the precipitating material to exert a mechanical stress on the reacting grain, and cause fracturing, when precipitation is confined within dissolution pits and wedges as illustrated below.

Experimental works that demonstrate this include the replacement reactions: aragonite → calcite (Perdikouri et al. 2011), leucite → analcime (Putnis et al. 2007; Jamtveit et al. 2009),

scolecite → tobermorite (Dunkel and Putnis 2014), and olivine → serpentine (Malvoisin et al. 2012). All of these reactions are associated with a volume increase, and all of them produce fresh surface area by reaction-driven fracturing in unconfined hydrothermal experiments. Figure 7 shows the interface morphology formed during the replacement of the zeolite mineral scolecite ($CaAl_2Si_3O_{10} \cdot 3H_2O$) by tobermorite ($Ca_5Si_6O_{17}(OH)_2 \cdot 5H_2O$) after 3 days in a 2M-NaOH solution at 200 ℃ (Dunkel and Putnis 2014). During the replacement, tobermorite precipitates in dissolution pits formed at the scolecite surface. These pits develop into wedge-shaped cavities. When fibrous tobermorite grows from the supersaturated solution towards the scolecite 'walls', it exerts a stress on them, and the tips of the wedge-shaped pits act as stress concentrators and drive the growth of fractures into the parent phase. These fractures expose fresh reactive surfaces, which allow the process to repeat itself.
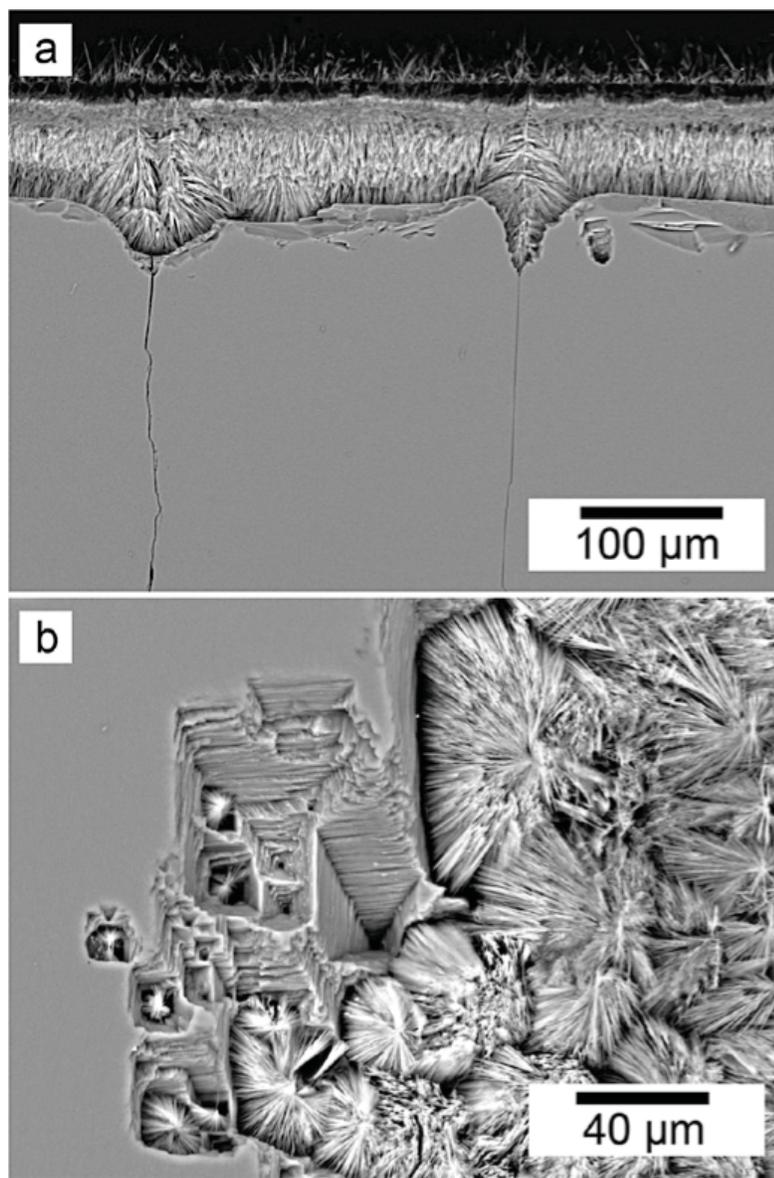
Figure 7. Scolecite reacting to form tobermorite. a) Fractures into scolecite emanating from dissolution-controlled, wedge-shaped depressions on the scolecite surface. b) Radial growth of fibrous tobermorite precipitating in etch pits formed on the reacting scolecite surface. [Modified from Dunkel and Putnis 2014.]

A similar process has been shown to operate during serpentinization of olivine. The interface between olivine and the hydrated product is always sharp, even at the nanometer scale. However, the interface is always rough with extensive pitting during incipient olivine dissolution. An amorphous proto-serpentine phase precipitates in these pits and causes local stress concentration and fracturing (Plümper et al. 2012). Pitting thus prepares fracturing during serpentinization, in a way similar to the case for the scolecite–tobermorite replacement reaction. When fracturing starts, the permeability of the system increases and when water gains access to fresh fracture surfaces, more pits are formed by dissolution, allowing new fractures to nucleate and grow producing the observed hierarchical fracture pattern associated with the commonly observed mesh texture that form during partial serpentinization of olivine crystals.

The examples above describe growth in cavities produced by dissolution processes that are directly coupled to local precipitation. In the following, we will examine reaction effects on the porosity and permeability of a medium with a significant initial porosity.

Growth in pores

If a fluid that flows through a network of pores becomes supersaturated with respect to a solid phase due to dissolution of reactive minerals, changes in temperature or pressure, or for any other reason, precipitation may take place in the open pore space.

If pores become filled with solid material, this will reduce the permeability of the rock. However, when the driving force for crystallization, i.e., the supersaturation or undercooling of the fluid phase, is sufficiently high, it will be energetically favorable for the system to continue precipitation of solid material even after the crystal has grown to fill its available pore space. By exerting a mechanical stress on the pore wall transmitted through the disjoining pressure of the confined-fluid film, the growing crystal can make the pore expand elastically and thus make room for continued growth. If stresses become high enough, this will cause fractures to form, and thus new fluid pathways are opened (Fig. 8).

Fracturing caused by the pressure exerted by mineral growth in porous rocks is a serious issue in a broad range of Earth and Environmental sciences, including conservation science, geomorphology, geotechnical engineering, and concrete materials science (Scherer 1999; Flatt et al. 2014).

The ability of growing crystals to lift imposed loads has been demonstrated in classical experiments (Becker and Day 1905; Correns 1949); see also Flatt et al. (2007) and Taber (1916, 1929). Crystallization pressures that exceed local failure thresholds are thought to be the key process responsible for the evolution of damage during salt weathering (Scherer 1999; Espinosa Marzal and Scherer 2008), frost heave in soils (Dash et al. 2006), and frost cracking of rocks (Walder and Hallet 1985; Murton et al. 2006). It may also lead to vein formation (Fletcher and Merino 2001; Røyne et al. 2011b) and displacive fabrics in the neighboring minerals (Watts 1978).

A crystal growing in a pore will stop growing when the stress on the crystal surface approaches the maximum crystallization pressure. However, if the stress is sufficient to open a fracture, the stress on the crystal surface will decrease, thus enabling further growth. When strain rates are slow, as can be the case during precipitation in pores and cracks, fracture propagation takes place through a kinetic process known as subcritical crack growth (Atkinson 1987). Røyne et al. (2011b) showed how to couple the rates of crystal growth and fracture propagation when a crystal grows from a supersaturated solution inside the aperture of a fracture (see Fig. 9). As long as there is an unlimited supply of supersaturated solution, fracture propagation causes the stress on the crystal surface to decrease and the rate of fracture propagation will accelerate until complete failure takes place.
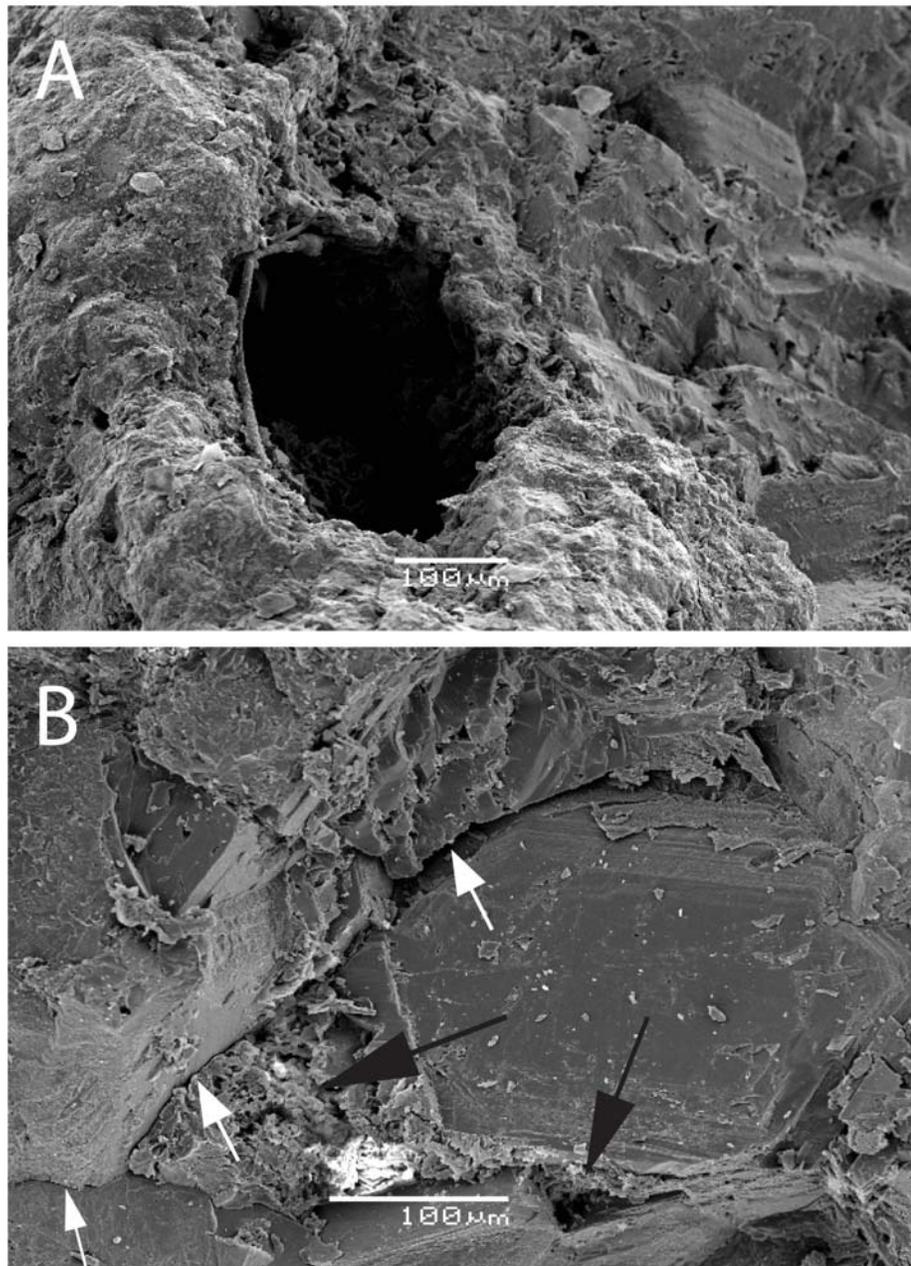
Figure 8. Secondary electron image of the surface of fresh (A) and weathered (B) andesite. Note the large subspherical pore in A. Dark arrows in B indicate inferred pre-existing pores that are now filled with a fine grained mixture of ferrihydrite and calcite. White arrows indicate microfractures at grain boundaries, inferred to have formed during growth in the pre-existing pores [Used with permission from John Wiley and Sons, from Jamtveit B, Kobchenko M, Austrheim H, Malthe-Sorenssen A, Røyne A, Svensen H (2011) Porosity evolution and crystallization-driven fragmentation during weathering of andesite, *Journal of Geophysical Research-Solid Earth*, Vol. 116, B12201, Fig. 5.]
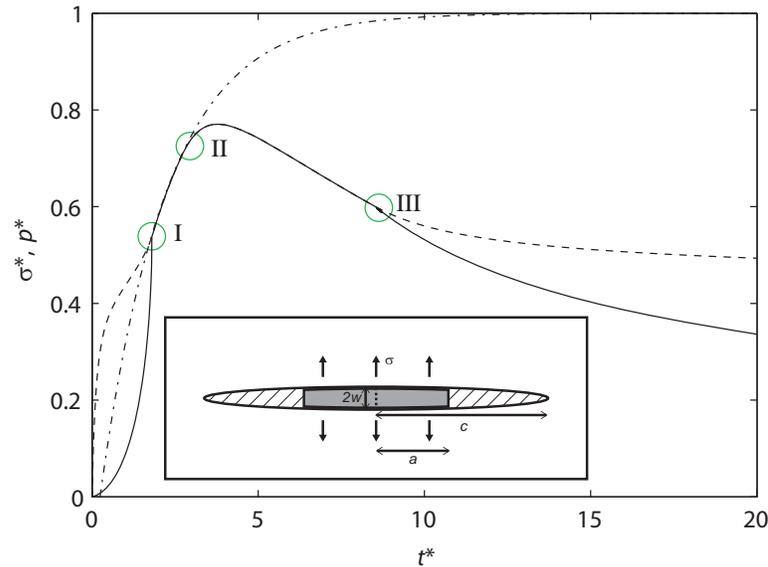
Figure 9. Insert: Conceptual model of a crystal (of radius *a*) growing in the aperture of a penny-shaped fracture (radius *c*, maximum opening *w*). A confined-fluid film between the crystal surface and the fracture walls sustains the continued crystal growth as long as the normal stress, σ, is smaller than the maximum disjoining pressure of the fluid film. Graph: Dimensionless normal stress on the crystal surface (normalized to the maximum crystallization pressure: dashed line) and equivalent pressure (the fluid pressure inside the penny-shaped fracture that would create the same driving force for fracture propagation: solid line) as a function of dimensionless time for a given set of crystal growth and fracture propagation parameters. The dash-dot line shows the stress on the crystal face that would develop if fracture propagation had not initiated at point II. At I, the crystal has grown to fill the entire fracture; at III, lateral crystal growth can no longer keep up with the fracture propagation rate, causing the stress on the crystal face to be larger than the equivalent fluid pressure. [Used with permission from Røyne A, Meakin P, Malthe-Sørenssen A, Jamtveit B, Dysthe DK (2011) Crack propagation driven by crystal growth. *EPL*, Vol. 96, 24003, doi:10.1209/0295-5075/96/24003].

In nature, the stress generated during crystal growth in the pores of a rock depends on the properties of the fluid film confined between the crystal surface and the pore wall as well as on the continued supply of supersaturated solution through transport in the fluid phase. We will discuss these issues in more details in the following two sections.

FUNDAMENTAL PROPERTIES OF CONFINED FLUID FILMS

As we have shown in the preceding sections, the processes that modify the porosity and permeability of rocks on the pore scale depend critically on the nature and presence of confined fluid films present in microfractures and along grain boundaries. When fluids are confined at reactive grain boundaries, they play a critical role in determining the force that is exerted by a growing crystal on its surroundings (Taber 1916; Espinosa Marzal and Scherer 2008) and whether a stressed grain boundary will heal or remain open (Renard et al. 2012; Houben et al. 2013). Confined fluids form transport pathways through low-permeability rocks (Alcantar et al. 2003), and fluids at grain boundaries also control macroscopic elastic (Tutuncu and Sharma 1992; Schult and Shi 1997) and yield properties (Risnes and Flaageng 1999; Megawati et al. 2013). For rocks that are stressed near failure, fluids confined at fracture tips control the fracture propagation threshold (Clarke et al. 1986; Røyne et al. 2011a).

It is extremely difficult to make direct measurements of the properties of nanometer-thick fluid films between mineral grains, but there are elegant ways in which the effects of such confined films can be observed. One of the most simple, yet highly illustrative, examples is the experiment by Bouzid et al. (2011). A solution of NaCl was introduced in a micrometric glass capillary, open on both ends (Fig. 10). As water evaporated to the dry external atmosphere, the solution gradually became supersaturated with respect to halite. After some time, solid halite crystals nucleated on both air–liquid interfaces. The crystals continued to grow until they completely filled the capillary diameter, apparently clogging the tube.

The system was then left undisturbed for three months. At this point, the authors observed that a small bubble had formed inside the fluid that was trapped between the halite cylinders. Such vapor cavities, which had nucleated inside the bulk liquid, can only form when the pressure in the liquid has decreased substantially below zero.

Instead of the halite crystals completely shutting off the transport pathway between the fluid in the capillary and the outside atmosphere, a fluid film must have persisted between the crystal and the glass wall. Water could continue to evaporate from the surface of this film, continuously pulling water out from the reservoir inside. Despite the presence of the water film, the crystals were not mechanically free to move inwards; instead, the depletion of water caused the pressure of the trapped solution to decrease. The wetting of the halite–glass interface was strong enough to prevent the gas–liquid interface from receding towards the middle of the capillary. In due course, the bulk fluid inside the capillary became thermodynamically unstable, and nucleation of vapor-filled cavities occurred.

In summary, evaporation of water caused this, initially extremely simple, system to follow a complex pathway: 1) increased concentration of sodium chloride; 2) the first phase transition, with nucleation and growth of salt crystals in the regions of highest salt concentration, the air–water interfaces; 3) decrease in fluid pressure; and 4) the second phase transition, nucleation of a vapor bubble. Given the complexity that resulted from this very simple setup, it is no surprise that the coupling between transport and reactions on different scales may lead to a variety of patterns in geological systems.

Figure 10. Halite crystals (dark grey), trapping a saturated solution of NaCl (light grey) in which a vapor bubble has formed. Note that the space between the halite crystals and the walls of the capillary is highly exaggerated in order to illustrate the negative curvature of the air–liquid surface. [Modified from Bouzid et al. 2011.]

The disjoining pressure of confined fluid films

The example described above illustrates how fluid films can persist and allow slow fluid transport, even in systems that seem to be completely clogged. Importantly, fluid films can persist even when their confining surfaces are squeezed together with a significant pressure, due to externally imposed stress or due to the stress generated during growth of a mineral. We will now address the conditions that allow fluid films to persist under compressive stress, starting with the fundamental thermodynamics.

Because atoms that form part of the surface of a material have fewer neighbors than those in the bulk, there is an excess free energy associated with all surfaces, called the surface energy, γ, of the material. This is also the energy that needs to be added to the system in order to create one unit area of new surface.

The intrinsic surface energy of a material, γ_0, may be defined as the excess free energy per unit area of a surface under vacuum conditions. However, in most applications, a surface of one material will be interacting with another gas, fluid, or solid phase. The measurable quantity is then not the intrinsic surface energy of the material, but rather the interfacial energy of phases 1 and 2 in contact, γ_{12}.

The concept of interfacial energies allows us to analyze the thermodynamics of a fluid sandwiched between two solid surfaces. Consider a system consisting of two semi-infinite, parallel solid surfaces of materials 1 and 2, separated by a distance h in a fluid medium 3 (Fig. 11), with total interfacial energy $U(h)$. If the surface separation is large enough to prevent any interaction between the solid surfaces, the energy of the system is $U(\infty) = \gamma_{13} + \gamma_{23}$. Upon bringing the solids into dry contact, the energy becomes $U(0) = \gamma_{12}$.
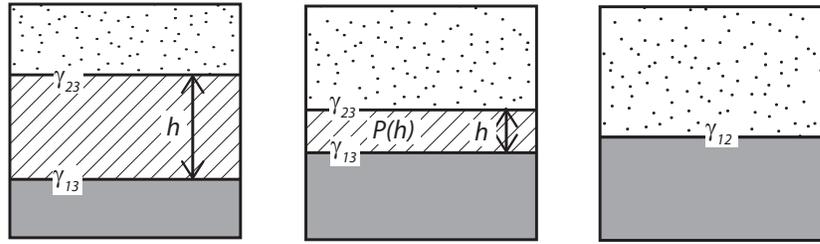
Figure 11. Surface energies and surface forces. Left: solid 1 and solid 2 separated by a thick film of liquid (3), $U(\infty) = \gamma_{13} + \gamma_{23}$. Right: solid–solid contact, with energy $U(0) = \gamma_{12}$. Middle: solids separated by a thin film, $U(h) = \gamma_{13} + \gamma_{23} + P(h)$.

As the film thickness decreases continually towards zero, the energy does not jump discontinuously from $\gamma_{13} + \gamma_{23}$ to γ_{12}. Instead, at sufficiently small separations, the interaction between the solid surfaces across the confined liquid film gives rise to an additional energy contribution, $P(h)$. We may then write the energy of the system as $U(h) = \gamma_{13} + \gamma_{23} + P(h)$, where $P(\infty) = 0$ and $P(0) = \gamma_{12} - (\gamma_{13} + \gamma_{23})$. When the surface separation changes, the change in interfacial energy gives rise to a measurable force per unit area:

$$\frac{F}{\ddot{}} = \frac{\mathrm{d}U(h)}{\mathrm{d}} = \frac{\mathrm{d}P(h)}{\mathrm{d}}. \tag{1}$$

This force, which may be attractive or repulsive, is referred to as a surface force. The corresponding pressure is called the disjoining pressure of the thin film (de Gennes et al. 2003; Israelachvili 2011). In the foregoing sections, where we have discussed the stability of fluid films, we have implicitly referred to repulsive disjoining pressures.

Forces between solids surfaces in a fluid medium arise from a number of processes, many of which are not yet properly understood. The most well-known theory, named DLVO theory after Derjaguin and Landau (1941) and Verwey and Overbeek (1948), contains two contributions to the surface forces. The first is the van der Waals force, which is a function of the polarizabilities of the materials involved, and is characterized by the Hamaker constant, A_H, of the interfacial system. Values for the Hamaker constant of a range of surfaces in air and water are available in the literature (Bergström 1997; Israelachvili 2011). For symmetric systems, where an interfacial layer separates two surfaces of the same material, the van der Waals force is always attractive, but for asymmetric systems, such as the ice–water–air

interface, it may be repulsive (Dash et al. 2006). For two flat surfaces, the van der Waals energy U_{vdW} is given by (Israelachvili 2011)

$$U_{vdW} = -\frac{A_H}{12\pi h^2}. \tag{2}$$

The corresponding force is given by the derivative of this function. Relations for other surface geometries are given in Israelachvili (2011).

The second contribution arises due to the overlap of the electric double layers associated with charged surfaces. Most solid surfaces become charged in liquid environments. The electric double layer interaction energy, U_{EDL}, between planar surfaces depends exponentially on the separation distance. For symmetric interfaces, monovalent electrolytes and surface potentials below about 25 mV, U_{EDL} can be found in terms of the surface potential ψ_0 or surface charge σ as (Israelachvili 2011):

$$U_{EDL} = \frac{2\varepsilon_0\varepsilon}{\lambda_D}\psi_0^2 e^{-h/\lambda_D} = \frac{2\lambda_D}{\varepsilon_0\varepsilon}\sigma^2 e^{-h/\lambda_D}. \tag{3}$$

Here, λ_D is the Debye screening length, which is a function of the ionic strength of the electrolyte. In pure water, λ_D is close to 1 μm, while in concentrated solutions it is on the order of a few tenths of a nanometer.

The DLVO theory has been experimentally validated using the Surface Forces Apparatus (SFA) (Israelachvili and Adams 1978; Israelachvili 2011), and more recently also with colloidal probe Atomic Force Microscopy (AFM) (Butt et al. 2005), in a range of systems. However, despite its advantages, the DLVO theory is not sufficient to predict the full interaction of a given pair of surfaces. One reason is that in high electrolyte concentrations, specific ion effects that are not accounted for in the DLVO framework become important (Boström et al. 2001). Also, even for moderate electrolyte concentration, one will need to know the surface charge or surface potentials; these are parameters that depend on the pH and ionic concentration of the pore fluid for any given mineral surface. There is a clear need for more data on this for geologically relevant systems, and progress is being made. Very recently, the atomic force microscope (AFM) has evolved to such an extent that it is possible to image the adsorption and dynamics of ions on a mineral surface (Ricci et al. 2013; Siretanu et al. 2014). This is giving us new insight into the complex processes of hydration and the electric double layer formation, and through this an exciting possibility to obtain a better understanding of wetting and surface interactions in geological systems.

At small separations, approaching a few molecular diameters, the continuum DLVO theory breaks down and other forces, that might be orders of magnitude larger than those described by DLVO, come into play. These forces depend on the molecular structure of the surfaces and intervening fluid, and include the hydrophobic attraction, hydration or hydrophilic repulsion, oscillatory solvation forces, ion correlation forces, and others (Israelachvili 2011). In geological systems, where large pressures can be expected, these forces may be the most important ones (Alcantar et al. 2003; Anzalone et al. 2006). Unfortunately, the theoretical framework for predicting these forces accurately is still lacking (although semi-empirical relations exist for specific cases such as hydrophobic attraction and hydration repulsion (Donaldson et al. 2014)).

Only more recently has attention been turned to high electrolyte concentrations. These systems are more complex, but their behavior is still consistent with the molecular picture that has been obtained for the lower solution concentrations (Baimpos et al. 2014). Interestingly, at these concentrations adhesive interaction forces are found to be largely due to solute

and solvent correlation forces (Lesko et al. 2001; Espinosa-Marzal et al. 2012; Baimpos et al. 2014). Ion correlation forces have been suggested to play a key role in controlling the cohesion of cement (Lesko et al. 2001), and we may speculate that they are a critical factor in determining the cohesive properties of natural rocks as well.

Transport in confined fluid films

When confined films become very thin, fluid and molecular transport becomes highly surface specific. The fluid viscosity may approach that of a solid-like material (Ruths and Israelachvili 2010), while on the other hand, diffusive ion transport may be significantly enhanced (Duan and Majumdar 2010). For thicker films, it is possible to make some generalizations about their properties. For instance, experiments typically show that the viscosity of a confined aqueous fluid film does deviate significantly from the bulk value until the film thickness is only a few molecular diameters (Horn et al. 1989). The diffusive properties of the film are also close to bulk values, and films as thin as 3–5 molecular diameters have been found to have a diffusivity that is less than one order of magnitude lower than that in bulk water (Alcantar et al. 2003). This implies that, in most cases, confined fluid films can be treated essentially as bulk fluids in terms of transport properties.

However, the large surface-to-fluid ratio of confined fluid films can give rise to surface- or fluid-specific properties that should not be ignored. For instance, the charge and wetting properties of the pore walls can significantly affect both advective and diffusive transport properties (Wang 2014). Since molecular species are affected in different ways by the properties of the pore walls, diffusion may cause individual species to become either depleted or enriched relative to that the bulk solution (Roach et al. 1988; Heidug 1995; Bresme and Cámara 2006).

Natural mineral interfaces typically display some degree of roughness on the nanoscale. If a normal force is applied across such a boundary it will lead to gradients in the disjoining pressure in the confined fluid. In this case, the process known as pressure diffusion can cause solutes of smaller molecular volume to flow in the direction of the pressure gradient, and therefore towards regions of decreasing grain boundary width where the disjoining pressure is large (Heidug 1995).

Because of the complexity of reaction-driven fracturing in geosystems, much remains to be understood and discovered. Nanoscale experiments and modeling will play an important role in the development of a comprehensive understanding of the coupling between dissolution, precipitation, and transport, as well as how these processes are coupled with deformation and fracturing.

INTERFACE-DRIVEN TRANSPORT ON THE PORE SCALE

The transport of material through a rock is not governed by its pore structure and permeability alone, but also by the driving forces for fluid migration. In the systems that we are discussing here, flows driven by differences in interfacial energies form an important class of transport phenomena. We will first discuss flow driven by the contact between a wetting fluid and a non-wetting fluid or gas phase. This is important during weathering of rocks near the Earth's surface, but also during water flooding of oil reservoirs and CO_2 injection into saturated rocks. We limit the discussion here to a few cases that are particularly relevant for the coupling between transport and precipitation; a more comprehensive review on the physics of pore-scale multiphase and multicomponent transport has been given by Steefel et al. (2013).

The following can be applied to any system containing two immiscible fluids where one is more wetting than the other. The difference in wetting properties is a result of the difference in

Figure 12. Creeping of a saturated NaCl solution, first as a thin layer of crystals on the side of the beaker (left) followed by secondary creeping on the first structure that formed, leading to a porous mass of crystals (right). [Reprinted with permission from (Bouzid M, Mercury L, Lassin A, Matray JM (2011) Salt precipitation and trapped liquid cavitation in micrometric capillary tubes. *Journal of Colloid and Interface Science,* Vol. 360, p. 768–776, doi:10.1016/j.jcis.2011.04.095). Copyright (2011) American Chemical Society.]

solid–liquid interfacial energies, which are much smaller for wetting than for the non-wetting fluids. Where the two fluid phases and the solid phase meet, the angle between the surface of the solid and that of the wetting fluid will be close to zero degrees. When confined inside a narrow pore or slit, the geometry imposed by the walls will cause the surface of the wetting fluid to curve inwards with a radius given by the pore opening. The drive in the system to minimize surface area will then manifest itself as a capillary pressure, pulling the wetting liquid towards the interface. In a vertical capillary tube, the balance between the capillary pressure and gravity determines the height to which the fluid will rise inside the tube. In a water-wetting, oil-saturated reservoir rock, capillary pressure will pull the water into the pores of the rock and the oil will be pushed out. In the experiment of Bouzid et al. (2011), the substantially negative capillary pressure at the air-water interface at the exit of the halite–glass channel caused fluid to be pulled out of the fluid reservoir between the halite crystals.

While mineral growth in pores can severely restrict pressure-driven fluid flow, it can also, in some cases, accelerate interface-driven fluid transport. A good example of this is the phenomenon of creeping salts (van Enckevort and Los 2013). If a salt solution is left in an open beaker in the lab, then, for some salts, one can return days later and find a crust of salt crystals covering the walls of the beaker all the way to the top, sometimes even down on the other side of the beaker and onto the benchtop—with most of the liquid solution gone (see Fig. 12). What has happened is that salt crystals have precipitated at the location where supersaturation is reached first, which is at the contact line between the salt solution and the beaker wall. Because water readily wets the salt crystals, the salt solution will climb up to the top of the newly precipitated material, where it again becomes supersaturated due to evaporation, which leads to more precipitation. With time, a porous structure builds upwards, allowing the salt solution to climb out of the beaker. The upward fluid flow and enhanced evaporation that is created by this crystallization leads to accelerated drying of the salt solution. A similar effect has been shown for salt crystallization due to evaporation in a hydrophobic porous medium (Sghaier et al. 2014).

In the absence of free boundaries (fluid–gas or fluid–fluid interfaces), there is yet another interfacial driving force that may drive fluid transport in porous systems, and that is the thermomolecular flow, where a temperature gradient generates a gradient in the disjoining pressure. This is now understood to be the main driving mechanism for frost heave, which is

the displacive growth of ice lenses in porous soils (Wettlaufer and Worster 2006), and at least some instances of frost cracking of intact rocks (Murton et al. 2006). Although water expands when it freezes to ice, this is in most cases not sufficient to form fractures and the extents of frost heave that are observed in nature. Instead, water is supplied to the freezing front from unfrozen parts of the material by the thermomolecular flow, which causes fluid to flow from warmer to colder temperatures. The fluid flow and build-up of ice will cease when the pressure on the ice lens from the displaced overburden is enough to balance the thermomolecular pressure. It is this continued supply of water from neighboring parts of the material that creates sufficient volume expansion to create fractures and damage.

In the case of the ice lens, the freezing of ice acts as a sink, helping to sustain the fluid flow. A mineral that grows in a pore will also deplete the solute concentration around it and cause diffusion solute from the surrounding reservoir. If the supersaturation of the fluid was initially uniform, and crystal nucleation was to take place in all pores simultaneously, then the supersaturation would soon be consumed without any significant build-up of solid material. However, in sufficiently small pores, crystals may be inhibited from precipitating even at high levels of supersaturation. This is due to the energy penalty associated with the large surface-to-volume of crystals confined inside a small volume of a different material. As a rule of thumb, the solubility of a salt crystal in a pore increases significantly in pores that are below 1 μm in size (Steiger 2005b). In a rock that contains a distribution of small and large pores, the small pores may act as reservoirs for supersaturated or subcooled fluid that feed the growth of crystals in larger pores. The pore-size distribution and connectivity can therefore have an important effect on the spatial distribution of precipitated material (Emmanuel and Berkowitz 2007), as well as on the damage of the material due to crystallization pressures (Scherer 1999; Steiger 2005b).

CONCLUDING REMARKS

By zooming in from the field scale to the pore and interface scales, we have shown that whenever fluid-driven reactions involve positive volume changes, the reaction will be shut down unless some mechanism ensures continued supply of fluid to the reactive surfaces. This requires a percolating network of fluid channels.

Fluid supply is normally maintained through fractures or pore networks with apertures exceeding micrometer size. However, the transport to the reacting surfaces often takes place through nanometer-scale fluid films. These films can often sustain a significant normal stress without being squeezed out.

For reactions to generate new fractures, which is often necessary to get access to the interior of reacting grains or to grains that are embedded inside a tight matrix, a significant overstepping of the relevant reaction is required. When crystals precipitate from a supersaturated solution, the growth process may elastically displace the confining surfaces. When the elastic strain reaches some critical value, this can result in fracture growth and the opening of new fluid pathways. The energy needed for the creation of new surfaces is thus taken from the chemical energy available in the reaction.

Even without fracturing, the coupling between reaction and transport in porous reactive rocks is highly complex. In order to better understand what determines the rates of advance of reaction fronts, whether reactions will come to a halt or not, and the evolution of the permeability of the rock, we need a better understanding of forces, transport and reaction kinetics under nanoscale confinement.

ACKNOWLEDGMENTS

REFERENCES

Alcantar N, Israelachvili J, Boles J (2003) Forces and ionic transport between mica surfaces: implications for pressure solution. Geochim Cosmochim Acta 67:1289–1304, doi:10.1016/s0016-7037(02)01270-x

Anzalone A, Boles J, Greene G, Young K, Israelachvili J, Alcantar N (2006) Confined fluids and their role in pressure solution. Chem Geol 230:220–231, doi:10.1016/j.chemgeo.2006.02.027

Atkinson BK (ed) (1987) Fracture Mechanics of Rock. Academic Press, London

Baimpos T, Shrestha BR, Raman S, Valtiner M (2014) Effect of interfacial ion structuring on range and magnitude of electric double layer, hydration, and adhesive interactions between mica surfaces in 0.05–3 M Li(+) and Cs(+) electrolyte solutions. Langmuir 30:4322–4332, doi:10.1021/la500288w

Becker GF, Day AL (1905) The linear force of growing crystals. Proc Washington Acad Sci 8:283–288

Bergström L (1997) Hamaker constants of inorganic materials. Adv Colloid Interfac 70:125–169, doi:10.1016/s0001-8686(97)00003-1

Boström M, Williams D, Ninham B (2001) Specific Ion Effects: Why DLVO theory fails for biology and colloid systems. Phys Rev Lett 87, doi:10.1103/PhysRevLett.87.168103

Bouzid M, Mercury L, Lassin A, Matray JM (2011) Salt precipitation and trapped liquid cavitation in micrometric capillary tubes. J Colloid Interface Sci 360:768–776, doi:10.1016/j.jcis.2011.04.095

Bresme F, Cámara LG (2006) Computer simulation studies of crystallization under confinement conditions. Chem Geol 230:197–206, doi:10.1016/j.chemgeo.2006.02.025

Butt H-J, Cappella B, Kappl M (2005) Force measurements with the atomic force microscope: Technique, interpretation and applications. Surf Sci Rep 59:1–152, doi:10.1016/j.surfrep.2005.08.003

Chapman RW, Greenfield MA (1949) Spheroidal weathering of igneous rocks. Am J Sci 247:407–429

Clarke DR, Lawn BR, Roach DH (1986) The Role of Surface Forces in Fracture. *In*: Fracture Mechanics of Ceramics. Vol 8. Bradt RC, Evans AG, Hasselman DPH, Lange FF, (eds). Plenum Publishing Corporation, p 341–350

Correns CW (1949) Growth and dissolution of crystals under linear pressure. Discuss Faraday Soc 5:267–271

Dash JG, Rempel AW, Wettlaufer JS (2006) The physics of premelted ice and its geophysical consequences. Rev Mod Phys 78:695–741

de Gennes P-G, Brochard-Wyart F, Quéré D (2003) Capillarity and Wetting Phenomena: Drops, Bubbles, Pearls, Waves. Springer, New York

Derjaguin B, Landau L (1941) Theory of the stability of strongly charged lyophobic sols and of the adhesion of strongly charged particles in solutions of electrolytes. Prog Surf Sci 43:30–59, doi:10.1016/0079-6816(93)90013-l

Donaldson SH, Jr., Røyne A, Kristiansen K, Rapp MV, Das S, Gebbie MA, Lee DW, Stock P, Valtiner M, Israelachvili J (2014) Developing a general interaction potential for hydrophobic and hydrophilic interactions. Langmuir, doi:10.1021/la502115g

Duan C, Majumdar A (2010) Anomalous ion transport in 2-nm hydrophilic nanochannels. Nat Nanotechnol 5:848–852, doi:10.1038/nnano.2010.233

Dunkel KG, Putnis A (2014) Replacement and ion exchange reactions of scolecite in a high pH aqueous solution. Eur J Mineral 26:61–69

Emmanuel S, Berkowitz B (2007) Effects of pore-size controlled solubility on reactive transport in heterogeneous rock. Geophys Res Lett 34:L06404, doi:10.1029/2006gl028962

Espinosa Marzal RM, Scherer GW (2008) Crystallization of sodium sulfate salts in limestone. Environ Geol 56:605–621, doi:10.1007/s00254-008-1441-7

Espinosa-Marzal RM, Drobek T, Balmer T, Heuberger MP (2012) Hydrated-ion ordering in electrical double layers. Phys Chem Chem Phys 14:6085–6093, doi:10.1039/c2cp40255f

Flatt RJ, Steiger M, Scherer GW (2007) A commented translation of the paper by C.W. Correns and W. Steinborn on crystallization pressure. Environ Geol 52:221–237

Flatt RJ, Caruso F, Sanchez AM, Scherer GW (2014) Chemo-mechanics of salt damage in stone. Nat Commun 5:4823, doi:10.1038/ncomms5823

Fletcher RC, Brantley SL (2010) Reduction of bedrock blocks as corestones in the weathering profile: observations and model. Am J Sci 310:131–164

Fletcher RC, Merino E (2001) Mineral growth in rocks: Kinetic-rheological models of replacement, vein formation, and syntectonic crystallization. Geochim Cosmochim Acta 65:3733–3748

Fletcher RC, Buss HL, Brantley SL (2006) A spheroidal weathering model coupling porewater chemistry to soil thickness during steady-state denundation. Earth Planet Sci Lett 244:444–457

Gibbs JW (1876) On the equilibrium of heterogeneous substances. Trans Connecticut Acad 3:108–248

Heidug WK (1995) Intergranular solid-fluid phase-transformations under stress - the effect of surface forces. J Geophys Res-Solid Earth 100:5931–5940

Horn RG, Smith DT, Haller W (1989) Surface forces and viscosity of water measured between silica sheets. Chem Phys Lett 162:404–408

Houben ME, ten Hove A, Peach CJ, Spiers CJ (2013) Crack healing in rocksalt via diffusion in adsorbed aqueous films: Microphysical modelling versus experiments. Phys Chem Earth, Parts A/B/C 64:95–104, doi:10.1016/j.pce.2012.10.001

Hövelmann J, Austrheim H, Jamtveit B (2012) Microstructure and porosity evolution during experimental carbonation of a natural peridotite. Chem Geol 334:254–265, doi:10.1016/j.chemgeo.2012.10.025

Israelachvili J (2011) Intermolecular and Surface Forces. Academic Press, Amsterdam.

Israelachvili JN, Adams GE (1978) Measurement of forces between two mica surfaces in aqueous-electrolyte solutions in range 0–100 nm. J Chem Soc, Faraday Trans I 74:975–1001

Jamtveit B, Hammer Ø (2012) Sculpting of rocks by reactive fluids. Geochem Perspect 1:340–480

Jamtveit B, Malthe-Sørenssen A, Kostenko O (2008) Reaction enhanced permeability during retrogressive metamorphism. Earth Planet Sci Lett 267:620–627, doi:10.1016/j.epsl.2007.12.016

Jamtveit B, Putnis CV, Malthe-Sorenssen A (2009) Reaction induced fracturing during replacement processes. Contrib Mineral Petrol 157:127–133

Jamtveit B, Kobchenko M, Austrheim H, Malthe-Sorenssen A, Røyne A, Svensen H (2011) Porosity evolution and crystallization-driven fragmentation during weathering of andesite. J Geophys Res-Solid Earth 116:B12204, doi:10.1029/2011JB008649

Kelemen PB, Hirth G (2012) Force of crystallization during retrograde metamorphism: Olivine hydration and carbonation. Earth Planet Sci Lett 345:81–89

Lesko S, Lesniewska E, Nonat A, Mutin J-C, Goudonnet J-P (2001) Investigation by atomic force microscopy of forces at the origin of cement cohesion. Ultramicroscopy 86:11–21

Malvoisin B, Brunet F (2014) Water diffusion-transport in a synthetic dunite: Consequences for oceanic peridotite serpentinization. Earth Planet Sci Lett 403:263–272, doi:10.1016/j.epsl.2014.07.004

Malvoisin B, Brunet F, Carlut J, Roumejon S, Cannat M (2012) Serpentinization of oceanic peridotites: 2. Kinetics and processes of San Carlos olivine hydrothermal alteration. J Geophys Res-Solid Earth 117, doi:10.1029/2011jb008842

Megawati M, Hiorth A, Madland MV (2013) The impact of surface charge on the mechanical behavior of high-porosity chalk. Rock Mech Rock Eng 46:1073–1090

Molnar P, Anderson RS, Anderson SP (2007) Tectonics, fracturing of rock, and erosion. J Geophys Res 112:F03014, doi:10.1029/2005jf000433

Murton JB, Peterson R, Ozouf J-C (2006) Bedrock fracture by ice segregation in cold regions. Science 314:1127–1129, doi:10.1126/science.1132127

Perdikouri C, Kasioptas A, Geisler T, Schmidt BC, Putnis A (2011) Experimental study of the aragonite to calcite transition in aqueous solution. Geochim Cosmochim Acta 75:6211–6224

Plümper O, Røyne A, Magraso Sola A, Jamtveit B (2012) The interface-scale mechanism of reaction-induced fracturing during upper mantle serpentinization. Geology 40:1103–1106

Prieto M, Cubillas P, Fernandez-Gonzalez A (2003) Uptake of dissolved Cd by biogenic and abiogenic aragonite: a comparison with sorption onto calcite. Geochim Cosmochim Acta 67:3857–3869

Putnis A (2002) Mineral replacement reactions: from macroscopic observations to microscopic mechanisms. Mineral Mag 66:689–708, doi:10.1180/0026461026650056

Putnis A (2015) Transient porosity resulting from fluid–mineral interaction and its consequences. Rev Mineral Geochem 80:1–23

Putnis CV, Geisler T, Schmid-Beurmann P, Stephan T, Giampaolo C (2007) An experimental study of the replacement of leucite by analcime. Am Mineral 92:19–26, doi:10.2138/am.2007.2249

Renard F, Beauprêtre S, Voisin C, Zigone D, Candela T, Dysthe DK, Gratier J-P (2012) Strength evolution of a reactive frictional interface is controlled by the dynamics of contacts and chemical effects. Earth Planet Sci Lett 341–344:20-34, doi:10.1016/j.epsl.2012.04.048

Ricci M, Spijker P, Stellacci F, Molinari JF, Voitchovsky K (2013) Direct visualization of single ions in the Stern layer of calcite. Langmuir 29:2207–2216, doi:10.1021/la3044736

Risnes R, Flaageng O (1999) Mechanical properties of chalk with emphasis on chalk–fluid interactions and micromechanical aspects. Oil Gas Science Tech 54:751–758

Roach DH, Lathabai S, Lawn BR (1988) Interfacial layers in brittle cracks. J Am Ceram Soc 71:97–105

Røyne A, Jamtveit B, Mathiesen J, Malthe-Sørenssen A (2008) Controls on rock weathering rates by reaction-induced hierarchical fracturing. Earth Planet Sci Lett 275:364–369, doi:10.1016/j.epsl.2008.08.035

Røyne A, Bisschop J, Dysthe DK (2011a) Experimental investigation of surface energy and subcritical crack growth in calcite. J Geophys Res 116:B04204, doi:10.1029/2010jb008033

Røyne A, Meakin P, Malthe-Sørenssen A, Jamtveit B, Dysthe DK (2011b) Crack propagation driven by crystal growth. EPL (Europhys Lett) 96:24003, doi:10.1209/0295-5075/96/24003

Rudge JF, Kelemen PB, Spiegelman M (2010) A simple model of reaction-induced cracking applied to serpentinization and carbonation of peridotite. Earth Planet Sci Lett 291:215–227

Ruths M, Israelachvili JN (2010) Surface Forces and Nanorheology of Molecularly Thin Films. *In*: Springer Handbook of Nanotechnology. Bhushan B (ed) Springer Berlin Heidelberg, pp. 857–922

Scherer GW (1999) Crystallization in pores. Cem Concr Res 29:1347–1358

Schult A, Shi G (1997) Hydration swelling of crystalline rocks. Geophys J Int 131:179–186

Sghaier N, Geoffroy S, Prat M, Eloukabi H, Ben Nasrallah S (2014) Evaporation-driven growth of large crystallized salt structures in a porous medium. Phys Rev E 90, doi:10.1103/PhysRevE.90.042402

Siretanu I, Ebeling D, Andersson MP, Stipp SL, Philipse A, Stuart MC, van den Ende D, Mugele F (2014) Direct observation of ionic structure at solid-liquid interfaces: a deep look into the Stern Layer. Sci Rep 4:4956, doi:10.1038/srep04956

Steefel CI, Molins S, Trebotich D (2013) Pore scale processes associated with subsurface CO_2 injection and sequestration. Rev Mineral Geochem 77:259–303

Steiger M (2005a) Crystal growth in porous materials—I: The crystallization pressure of large crystals. J Cryst Growth 282:455–469

Steiger M (2005b) Crystal growth in porous materials—II: Influence of crystal size on the crystallization pressure. J Cryst Growth 282:470–481

Taber S (1916) The growth of crystals under external pressure. Am J Sci 41:532–556

Taber S (1929) Frost heaving. J Geol 37:428–461

Tutuncu AN, Sharma MM (1992) The influence of fluids on grain contact stiffness and frame moduli in sedimentary rocks. Geophysics 57:1571–1582

Ulven OI, Jamtveit B, Malthe-Sørenssen A (2014a) Reaction driven fracturing of porous rocks. J Geophys Res:doi:10.1002/2014JB011102

Ulven OI, Storheim H, Austrheim H, Malthe-Sørenssen A (2014b) Fracture initiation during volume increasing reactions in rocks and applications for CO_2 sequestration. Earth Planet Sci Lett 389:132–142, doi:10.1016/j.epsl.2013.12.039

van Enckevort WJP, Los JH (2013) On the creeping of saturated salt solutions. Cryst Growth Des 13:1838–1848, doi:10.1021/cg301429g

Verwey EJW, Overbeek JTG (1948) Theory of The Stability of Lyophobic Colloids. Elsevier, Amsterdam

Walder J, Hallet B (1985) A theoretical-model of the fracture of rock during freezing. Geol Soc Am Bull 96:336–346

Wang Y (2014) Nanogeochemistry: Nanostructures, emergent properties and their control on geochemical reactions and mass transfers. Chem Geol 378-379:1-23, doi:10.1016/j.chemgeo.2014.04.007

Watts NL (1978) Displacive calcite: Evidence from recent and ancient calcretes. Geology 6:699–703

Wettlaufer JS, Worster MG (2006) Premelting dynamics. Annu Rev Fluid Mech 38:427–452